

Supplement of Atmos. Chem. Phys., 16, 2943–2970, 2016
<http://www.atmos-chem-phys.net/16/2943/2016/>
doi:10.5194/acp-16-2943-2016-supplement
© Author(s) 2016. CC Attribution 3.0 License.



Atmospheric
Chemistry
and Physics
Open Access
EGU

Supplement of

In situ secondary organic aerosol formation from ambient pine forest air using an oxidation flow reactor

Brett B. Palm et al.

Correspondence to: Jose L. Jimenez (jose.jimenez@colorado.edu)

The copyright of individual parts of the supplement might differ from the CC-BY 3.0 licence.

1 **S1 Correction for particle diffusion to sampling line walls**

2 AMS and SMPS particle concentrations were corrected for diffusion losses to the walls of the inlet
3 sampling lines, estimated using the Max Planck Institute for Chemistry's Particle Loss Calculator (von der
4 Weiden et al., 2009). The sampling lines were constructed from a mixture of 3/8" and 1/4" OD copper
5 tubing. The ambient air sampling line contained a PM_{2.5} cyclone impactor at the inlet. The total length of
6 tubing between the cyclone/OFR and AMS/SMPS was approximately 8 m, with a total residence time of
7 about 9 s. The transmission curve used to correct for line losses is shown in Fig. S1. Estimates for particle
8 losses in the ambient sampling line and in the OFR sampling line were similar, so a single transmission
9 curve is applied to all data. The transmission curve was applied to SMPS size distributions to determine
10 particle volume lost to the inlet walls. This volume was added to the AMS species in the same ratio that
11 the species volumes were measured by the AMS. As seen in Fig. S1, there was on average only a slight
12 size dependence to the species mass fractions of ambient aerosol. The mass fractions are also
13 particularly noisy at smaller particle sizes due to small mass concentrations. Ideally, the species size
14 distributions measured at each point in time could be used to allocate the sampling line particle losses
15 to each species. In practice, the AMS size-distribution measurement mode is not sensitive enough at
16 these concentrations to do such a correction at high time-resolution. Ambient AMS size distribution data
17 could be averaged over long periods of time to increase the signal-to-noise, but this would not be
18 possible for OFR measurements, since the OH exposure is changed between each successive data point.
19 Thus, we have applied the best correction possible and expect that it should improve quantification.
20 Regardless, the small size dependence of species mass fractions would have a minimal impact on this
21 analysis since the correction is at most 20% at the smallest sizes. Mass was estimated from volume using
22 densities of 1.52 g cm⁻³ for chloride and 1.75 g cm⁻³ for sulfate, ammonium, and nitrate AMS aerosol
23 species (DeCarlo et al., 2004; Salcedo et al., 2006; Lide, 2013), and a parameterization using elemental
24 composition to estimate the density of OA (Kuwata et al., 2012). The combination of the sampling line
25 particle loss correction and the AMS lens transmission correction (discussed in Sect. S3) added an
26 average of 4% to the ambient OA, and an average of 12% to the OA measured after 0.4–1.5 days of
27 aging (when the corrections were largest).

28 **S2 Determination of AMS collection efficiency (CE)**

29 CE is typically variable between 0.5 and 1, depending on composition, as detailed in Middlebrook et al.
30 (2012). To our knowledge, ambient AMS measurements with a constant CE of ~1 have been reported in
31 two prior studies in forested environments: during the wet season in the remote Amazon forest at the

32 Amazonian Aerosol Characterization Experiment 2008 (Chen et al., 2015), and South American Biomass
33 Burning Analysis (SAMBBA) experiment during the dry season and dry-to-wet transition period in the
34 southwestern Amazon rainforest in 2012 (Brito et al., 2014). Here, we assessed CE by comparing AMS
35 measurements with an SMPS that sampled from the same inlet. This SMPS measurement was validated
36 by an intercomparison with four other calibrated and independently-operated SMPS instruments, as
37 well as three CPC total particle number measurements, that sampled concurrently at the same research
38 site. Fig. S2 shows that $CE = 1$ was required to match the AMS and SMPS measurements.

39 One concern was that the CE would change after oxidation in the OFR, due to changes in the aerosol
40 composition and properties. A change in CE would result in a change in the slope of AMS vs. SMPS
41 volume. However, we did not observe such a change, as seen in the comparison of total aerosol volume
42 measured after the OFR in the left panel of Fig. S3. Occasionally, high concentrations of NH_4NO_3 were
43 produced in the OFR from OH oxidation. During those times, the AMS measured up to several times
44 more volume than the SMPS (implying a $CE \gg 1$). This is likely due to evaporation of the NH_4NO_3 in the
45 SMPS, as the SMPS sample flow was diluted inside the DMA column, as well as between the DMA and
46 the CPC. For this reason, these data are not included in the analysis of CE.

47 Fig. S4 shows total particle volume enhancements as quantified by both the AMS and the SMPS for the
48 OFR185 method vs. photochemical age, split into daytime and nighttime, showing that the two
49 instruments measured similar enhancements within the errors at all ages. Data in Figs. S2, S3, and S4
50 were corrected using the sampling inlet line particle transmission efficiency curve in Fig. S1 as well as a
51 correction for the transmission of the AMS aerodynamic lens, discussed in Sect. S3.

52 **S3 Determination of AMS aerodynamic lens transmission efficiency**

53 As discussed in Sect. 3.5 and Fig. 9, OH oxidation of ambient air in the OFR often led to substantial new
54 particle formation. The AMS aerodynamic lens is known to have less than 100% transmission at small
55 sizes (Liu et al., 2007). A standard transmission curve has been suggested for correcting AMS data when
56 lacking a determination of the transmission for the particular operating conditions of the AMS, referred
57 to as case 0 here (Knote et al., 2011). However, it is preferable to use data from a specific experiment
58 when available to make such a determination for specific operating conditions. The lens transmission
59 curve was estimated for the conditions in which the AMS was operated at the BEACHON-RoMBAS
60 campaign by empirically finding the low particle size cutoff that resulted in the highest R^2 correlation of
61 the AMS and SMPS total volume sampled through an OFR (including all data from unperturbed to the

62 highest OH_{exp}). We tested a range of corrections, shown in Fig. S5. The results are shown in Table S1.
63 Scatterplots of total volume and change in volume for the base case (no correction) and the chosen case
64 2 correction are shown in Figs. S6 and S3, respectively. The combination of the sampling line particle loss
65 correction and the AMS lens transmission correction added an average of 4% to the ambient OA, and an
66 average of 12% to the total OA measured after 0.4–1.5 days of aging in the reactor (when the
67 corrections were largest).

68 Finally, to account for any particle losses on the surfaces inside the OFR, the aerosol mass measured in
69 the OFR when no oxidant was added was adjusted to be equal to the concurrent ambient aerosol data,
70 which was interpolated from the measurements immediately before and after the OFR data. Aerosol
71 was sampled through the OFR with no added oxidant approximately every 2 hours. The OFR data for
72 which oxidant concentrations were increased were corrected by multiplying by the average ratio of
73 ambient aerosol mass to aerosol mass measured through the OFR without added oxidant. This
74 correction was small, increasing the mass of OFR data by 4%, similar in magnitude to the loss of particles
75 in the sampling lines and aerodynamic lens.

76 **S4 In-canopy vs. 25 m height PTR-TOF-MS measurements**

77 The primary PTR-TOF-MS dataset from BEACHON-RoMBAS was measured from an inlet located on a
78 tower at 25 m, above the average canopy height of 16 m (Ortega et al., 2014). The OFR was located
79 within the canopy at approximately 4 m height. Occasionally, concurrent PTR-TOF-MS measurements
80 were available from the 25 m height and either through the OFR (1–6 and 8–10 August) or from a 1 m
81 high inlet (19–21 August). Scatterplots of in-canopy (OFR or 1 m) vs. 25 m inlet MT, SQT, MBO+isoprene,
82 and toluene+*p*-cymene concentrations are shown in Fig. S8. In-canopy concentrations were observed to
83 be 1.9, 5.9, 1.4, and 1.2 times higher than at 25 m for those four compounds, respectively, and these
84 ratios were used to estimate a campaign-long time series of in-canopy concentrations using the 25 m
85 measurements. The correlations are high for MT, toluene, and MBO+isoprene ($R^2=0.80-0.82$), but the
86 correlation for SQT is $R^2=0.12$. This low correlation adds uncertainty to the estimation of in-canopy SQT
87 concentrations. However, this will have only a minor effect on the predicted SOA formation from VOCs
88 (Sect. 3.6.1) since on average only 5% of the predicted SOA formation came from SQT.

89

90 **References**

- 91 Brito, J., Rizzo, L. V., Morgan, W. T., Coe, H., Johnson, B., Haywood, J., Longo, K., Freitas, S., Andreae, M.
92 O. and Artaxo, P.: Ground-based Aerosol Characterization During The South American Biomass Burning
93 Analysis (SAMBBA) Field Experiment, *Atmos. Chem. Phys.*, 14, 12069–12083, doi:10.5194/acp-14-12069-
94 2014, 2014.
- 95 Chen, Q., Farmer, D. K., Rizzo, L. V., Pauliquevis, T., Kuwata, M., Karl, T. G., Guenther, A., Allan, J. D., Coe,
96 H., Andreae, M. O., Pöschl, U., Jimenez, J. L., Artaxo, P. and Martin, S. T.: Submicron Particle Mass
97 Concentrations And Sources In The Amazonian Wet Season (AMAZE-08), *Atmos. Chem. Phys.*, 15, 3687–
98 3701, doi:10.5194/acp-15-3687-2015, 2015.
- 99 DeCarlo, P. F., Slowik, J. G., Worsnop, D. R., Davidovits, P. and Jimenez, J. L.: Particle Morphology And
100 Density Characterization By Combined Mobility And Aerodynamic Diameter Measurements. Part 1:
101 Theory, *Aerosol Sci. Technol.*, 38, 1185–1205, doi:10.1080/027868290903907, 2004.
- 102 Knote, C., Brunner, D., Vogel, H., Allan, J., Asmi, A., Äijälä, M., Carbone, S., van der Gon, H. D., Jimenez, J.
103 L., Kiendler-Scharr, A., Mohr, C., Poulain, L., Prévôt, A. S. H., Swietlicki, E. and Vogel, B.: Towards An
104 Online-coupled Chemistry-climate Model: Evaluation Of Trace Gases And Aerosols In COSMO-ART,
105 *Geosci. Model Dev.*, 4, 1077–1102, doi:10.5194/gmd-4-1077-2011, 2011.
- 106 Kuwata, M., Zorn, S. R. and Martin, S. T.: Using Elemental Ratios To Predict The Density Of Organic
107 Material Composed Of Carbon, Hydrogen, And Oxygen., *Environ. Sci. Technol.*, 46, 787–94,
108 doi:10.1021/es202525q, 2012.
- 109 Lide, D. R.: *CRC Handbook Of Chemistry And Physics*, 94th Edition, 2013-2014, 2013.
- 110 Liu, P. S. K., Deng, R., Smith, K. a., Williams, L. R., Jayne, J. T., Canagaratna, M. R., Moore, K., Onasch, T.
111 B., Worsnop, D. R. and Deshler, T.: Transmission Efficiency Of An Aerodynamic Focusing Lens System:
112 Comparison Of Model Calculations And Laboratory Measurements For The Aerodyne Aerosol Mass
113 Spectrometer, *Aerosol Sci. Technol.*, 41, 721–733, doi:10.1080/02786820701422278, 2007.
- 114 Middlebrook, A. M., Bahreini, R., Jimenez, J. L. and Canagaratna, M. R.: Evaluation Of Composition-
115 Dependent Collection Efficiencies For The Aerodyne Aerosol Mass Spectrometer Using Field Data,
116 *Aerosol Sci. Technol.*, 46, 258–271, doi:10.1080/02786826.2011.620041, 2012.
- 117 Ortega, J., Turnipseed, A., Guenther, A. B., Karl, T. G., Day, D. A., Gochis, D., Huffman, J. A., Prenni, A. J.,
118 Levin, E. J. T., Kreidenweis, S. M., DeMott, P. J., Tobo, Y., Patton, E. G., Hodzic, A., Cui, Y. Y., Harley, P. C.,
119 Hornbrook, R. S., Apel, E. C., Monson, R. K., Eller, A. S. D., Greenberg, J. P., Barth, M. C., Campuzano-Jost,
120 P., Palm, B. B., Jimenez, J. L., Aiken, A. C., Dubey, M. K., Geron, C., Offenberg, J., Ryan, M. G., Fornwalt, P.
121 J., Pryor, S. C., Keutsch, F. N., DiGangi, J. P., Chan, A. W. H., Goldstein, A. H., Wolfe, G. M., Kim, S., Kaser,
122 L., Schnitzhofer, R., Hansel, A., Cantrell, C. A., Mauldin, R. L. and Smith, J. N.: Overview Of The Manitou
123 Experimental Forest Observatory: Site Description And Selected Science Results From 2008 To 2013,
124 *Atmos. Chem. Phys.*, 14, 6345–6367, doi:10.5194/acp-14-6345-2014, 2014.
- 125 Salcedo, D., Onasch, T. B., Dzepina, K., Canagaratna, M. R., Zhang, Q., Huffman, J. A., DeCarlo, P. F.,
126 Jayne, J. T., Mortimer, P., Worsnop, D. R., Kolb, C. E., Johnson, K. S., Zuberi, B., Marr, L. C., Volkamer, R.,
127 Molina, L. T., Molina, M. J., Cardenas, B., Bernabé, R. M., Márquez, C., Gaffney, J. S., Marley, N. A.,
128 Laskin, A., Shutthanandan, V., Xie, Y., Brune, W., Leshner, R., Shirley, T. and Jimenez, J. L.: Characterization
129 Of Ambient Aerosols In Mexico City During The MCMA-2003 Campaign With Aerosol Mass
130 Spectrometry: Results From The CENICA Supersite, *Atmos. Chem. Phys.*, 6, 925–946, doi:10.5194/acp-6-
131 925-2006, 2006.
- 132 Tsimpidi, A. P., Karydis, V. A., Zavala, M., Lei, W., Molina, L., Ulbrich, I. M., Jimenez, J. L. and Pandis, S. N.:

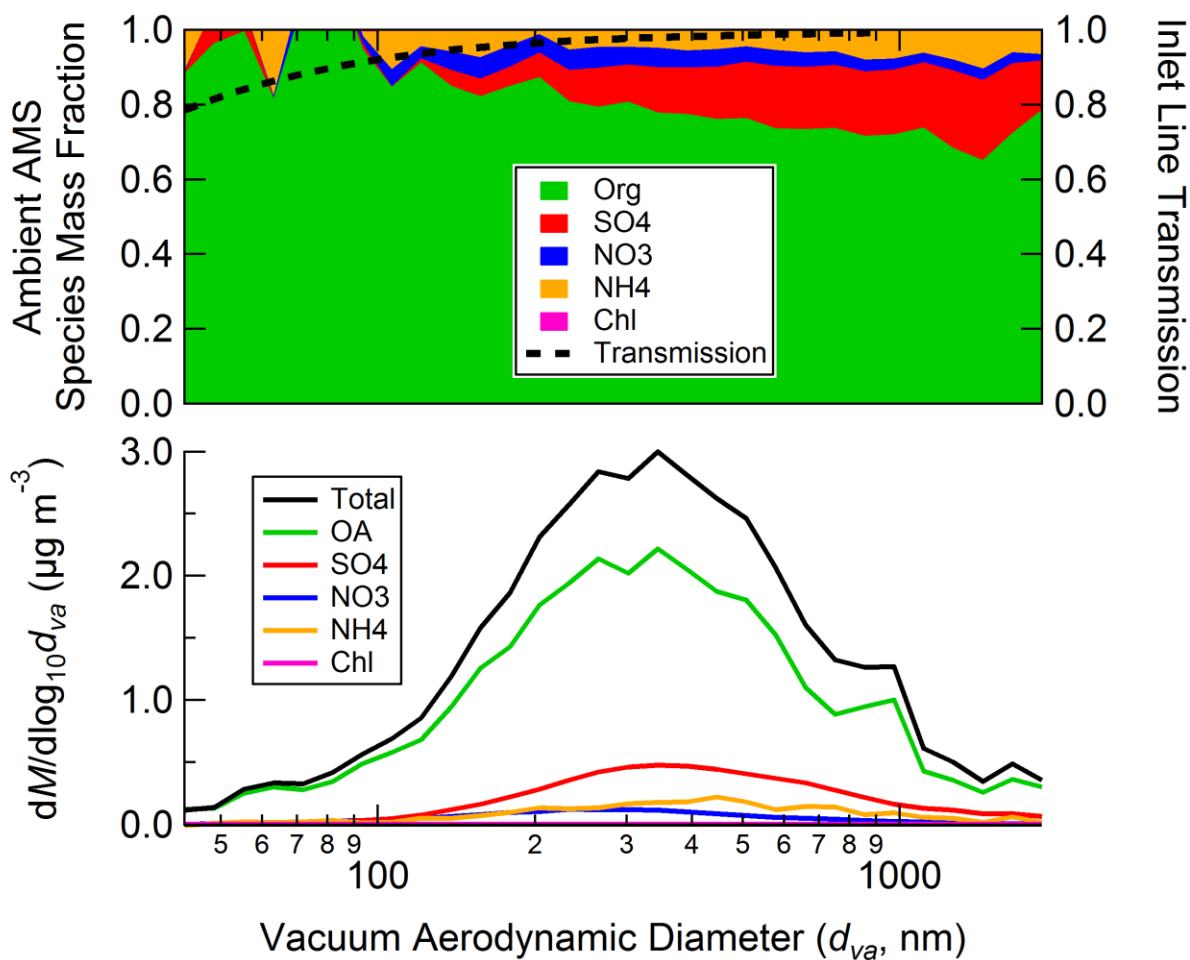
133 Evaluation Of The Volatility Basis-set Approach For The Simulation Of Organic Aerosol Formation In The
134 Mexico City Metropolitan Area, *Atmos. Chem. Phys.*, 10, 525–546, doi:10.5194/acp-10-525-2010, 2010.
135 von der Weiden, S.-L., Drewnick, F. and Borrmann, S.: Particle Loss Calculator – A New Software Tool For
136 The Assessment Of The Performance Of Aerosol Inlet Systems, *Atmos. Meas. Tech.*, 2, 479–494,
137 doi:10.5194/amt-2-479-2009, 2009.
138
139

140 Table S1. Slope and correlation values for a comparison of AMS vs. SMPS volume, when applying
141 aerodynamic lens transmission correction curves 0-5 (shown in Fig. S5) or no correction (base case).

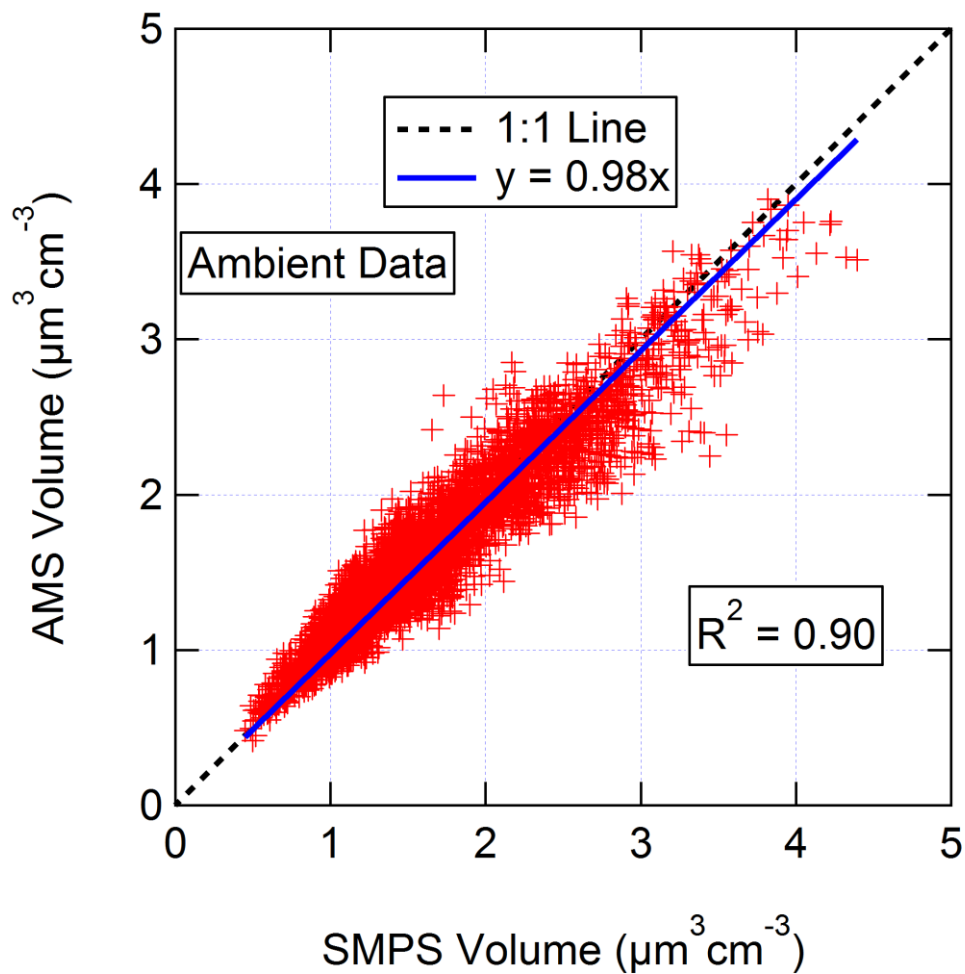
<u>Total Volume</u>			<u>Change in Volume</u>		
<u>Case</u>	<u>Slope</u>	<u>R²</u>	<u>Case</u>	<u>Slope</u>	<u>R²</u>
0	1.056	0.85	0	1.446	0.77
1	1.036	0.85	1	1.341	0.77
2	1.017	0.86	2	1.219	0.75
3	1.001	0.85	3	1.107	0.70
4	0.989	0.84	4	1.032	0.65
5	0.983	0.82	5	0.997	0.61
base	0.981	0.81	base	0.986	0.58

142

143



144
 145 **Fig. S1.** Top: Average species mass fraction of ambient aerosol measured by the AMS, and inlet sampling
 146 line particle transmission efficiency. The transmission efficiency was estimated using the Max Planck
 147 Institute for Chemistry Particle Loss Calculator (von der Weiden et al., 2009). This transmission curve
 148 was used to correct SMPS size distributions for particle losses in the ambient and OFR sampling lines.
 149 Particle losses to surfaces inside the OFR are discussed in Sect. S3. Bottom: Average species mass size
 150 distribution of ambient aerosol measured by the AMS.



151

152 Fig. S2. Scatter plot of ambient aerosol volume measurements from AMS vs. SMPS with regression line.

153 AMS data was calculated using CE=1. AMS volume was estimated using densities of 1.52 g cm^{-3} for

154 chloride, 1.75 g cm^{-3} for sulfate, ammonium, and nitrate (DeCarlo et al., 2004; Salcedo et al., 2006; Lide,

155 2013), and a parameterization using elemental composition to estimate the density of OA (Kuwata et al.,

156 2012). All data is shown without the LVOC fate correction.

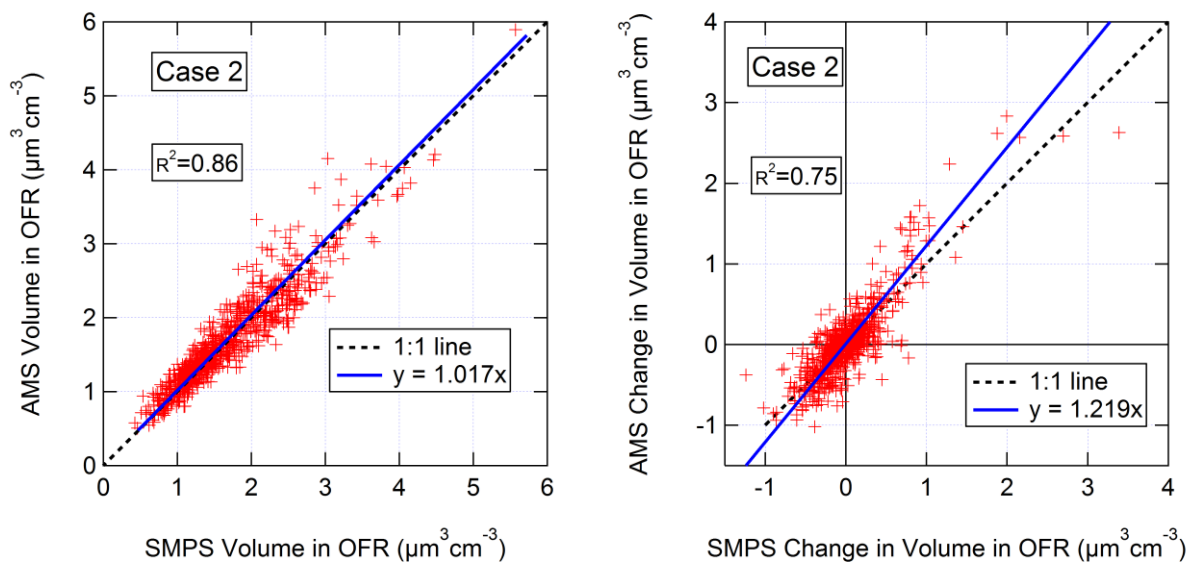
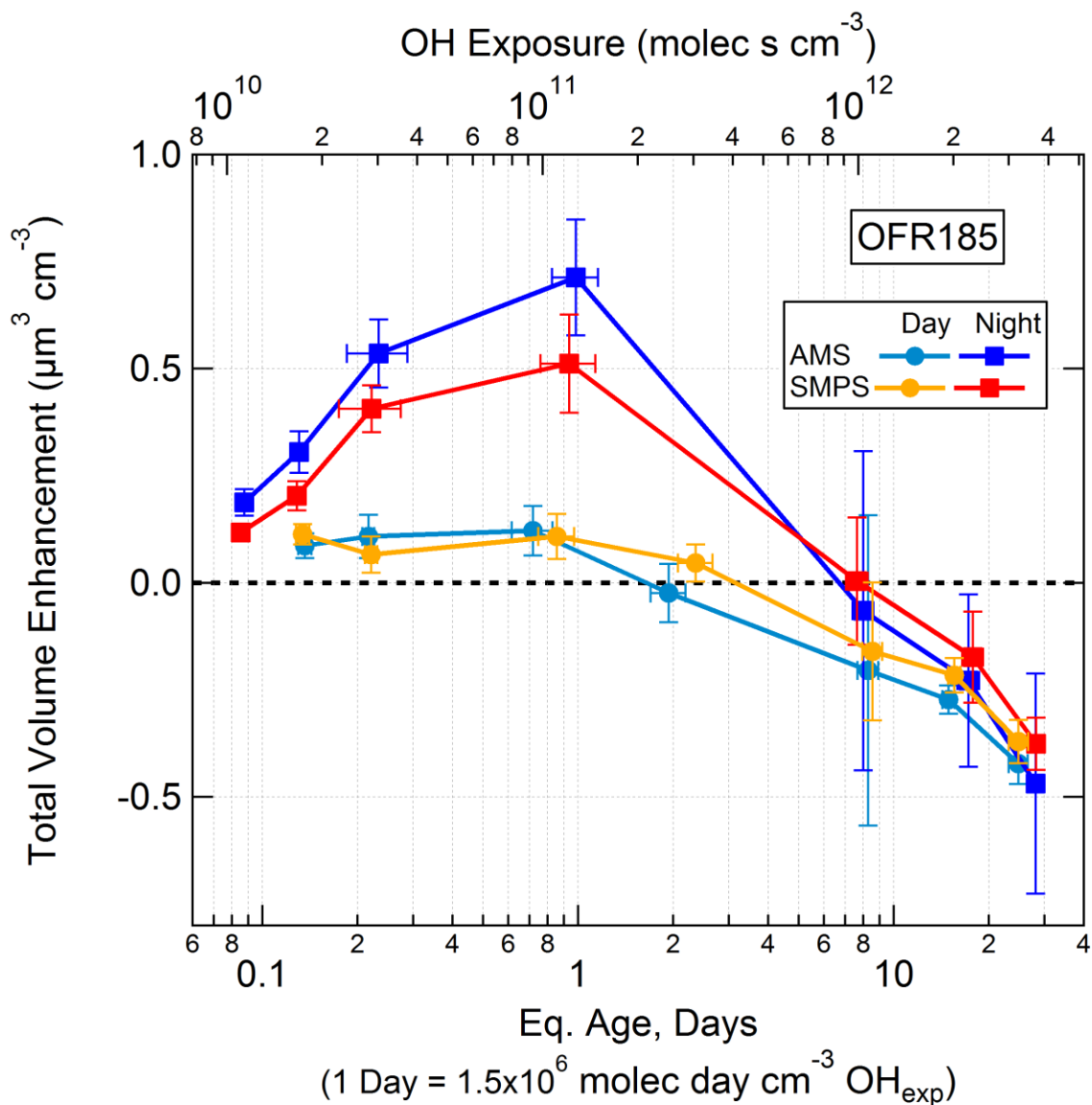


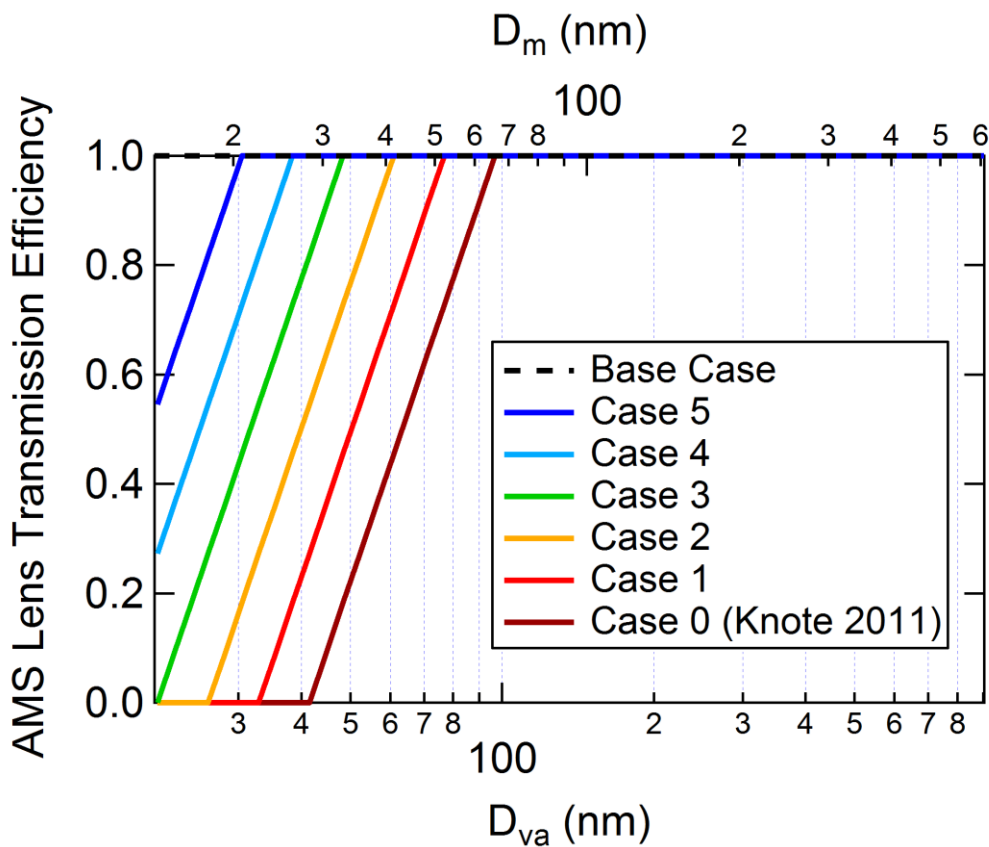
Fig. S3. Scatter plot of aerosol volume and change in volume after OH aging from AMS vs. SMPS. AMS volume was estimated using densities of 1.52 for chloride, 1.75 for sulfate, ammonium, and nitrate (DeCarlo et al., 2004; Salcedo et al., 2006; Lide, 2013), and a parameterization using elemental composition to estimate the density of OA (Kuwata et al., 2012). Data is shown after correction for particle transmission losses in the AMS aerodynamic lens according to the case 2 correction in Fig. S5. All data is shown without the LVOC fate correction. At the highest ages, heterogeneous oxidation led to fragmentation/volatilization of preexisting OA, resulting in a net loss of OA.



166

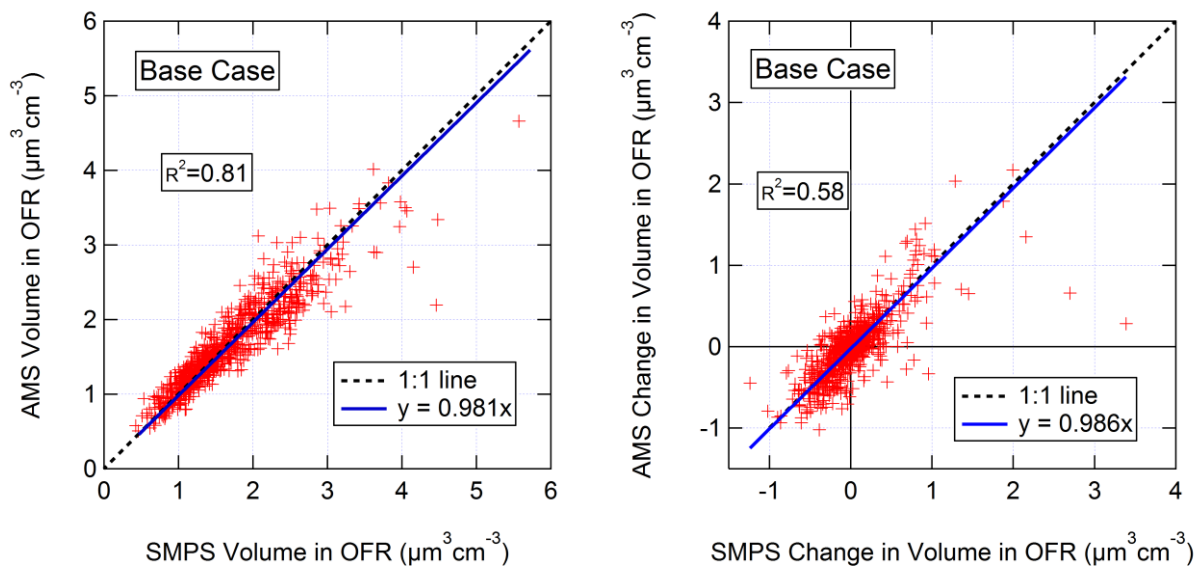
167 Fig. S4. Total particle volume enhancement as measured by the AMS and SMPS as a function of
 168 photochemical age, split into daytime (08:00–20:00 local time) and nighttime (20:00–08:00 local time)
 169 data. AMS volume was estimated using densities of 1.52 g cm^{-3} for chloride, 1.75 g cm^{-3} for sulfate,
 170 ammonium, and nitrate (DeCarlo et al., 2004; Salcedo et al., 2006; Lide, 2013), and a parameterization
 171 using elemental composition to estimate the density of OA (Kuwata et al., 2012). All data is shown
 172 without the LVOC fate correction. Error bars represent the standard error of the mean of each quantile
 173 of data.

174

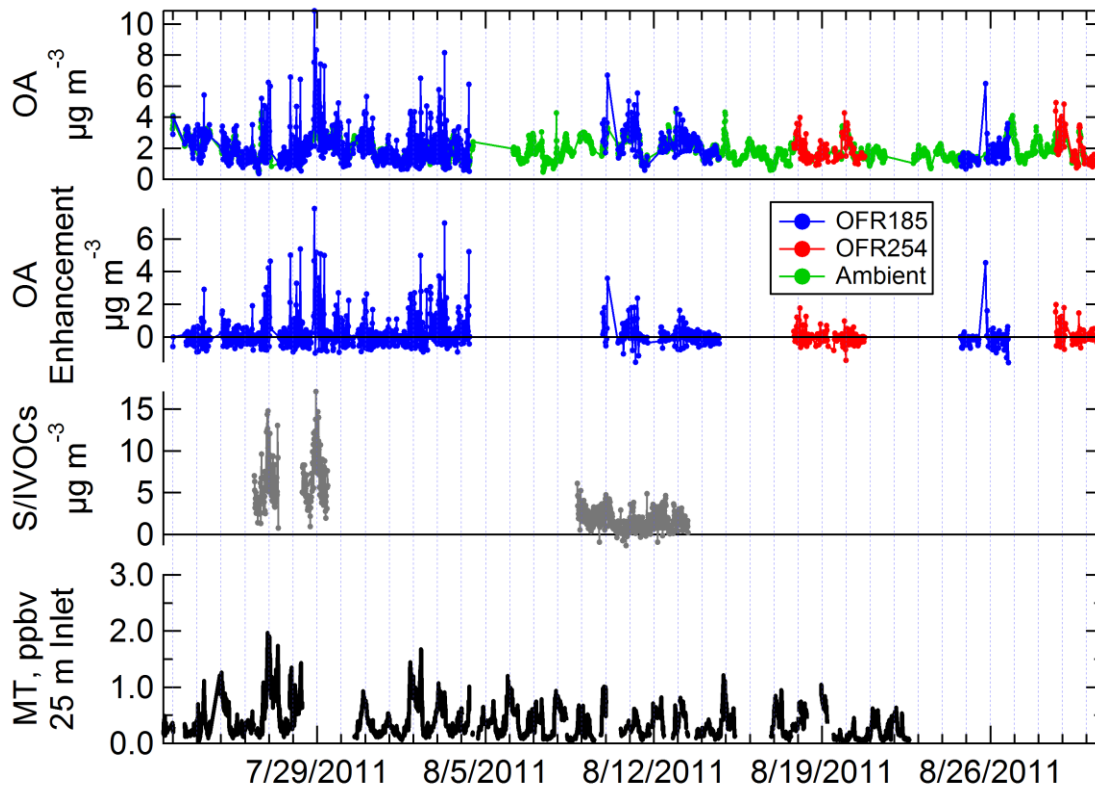


175

176 Fig. S5. Potential AMS aerodynamic lens transmission efficiency curves used to evaluate small particle
 177 losses in the lens, as a function of vacuum aerodynamic diameter D_{va} and mobility diameter D_m . D_{va} was
 178 converted to D_m assuming a density of 1.45 g cm^{-3} (the campaign average). Case 0 is the recommended
 179 AMS lens transmission efficiency when no campaign-specific determination is possible (Knote et al.,
 180 2011). Case 2 was chosen as the best fit for the data under the conditions during BEACHON-RoMBAS.



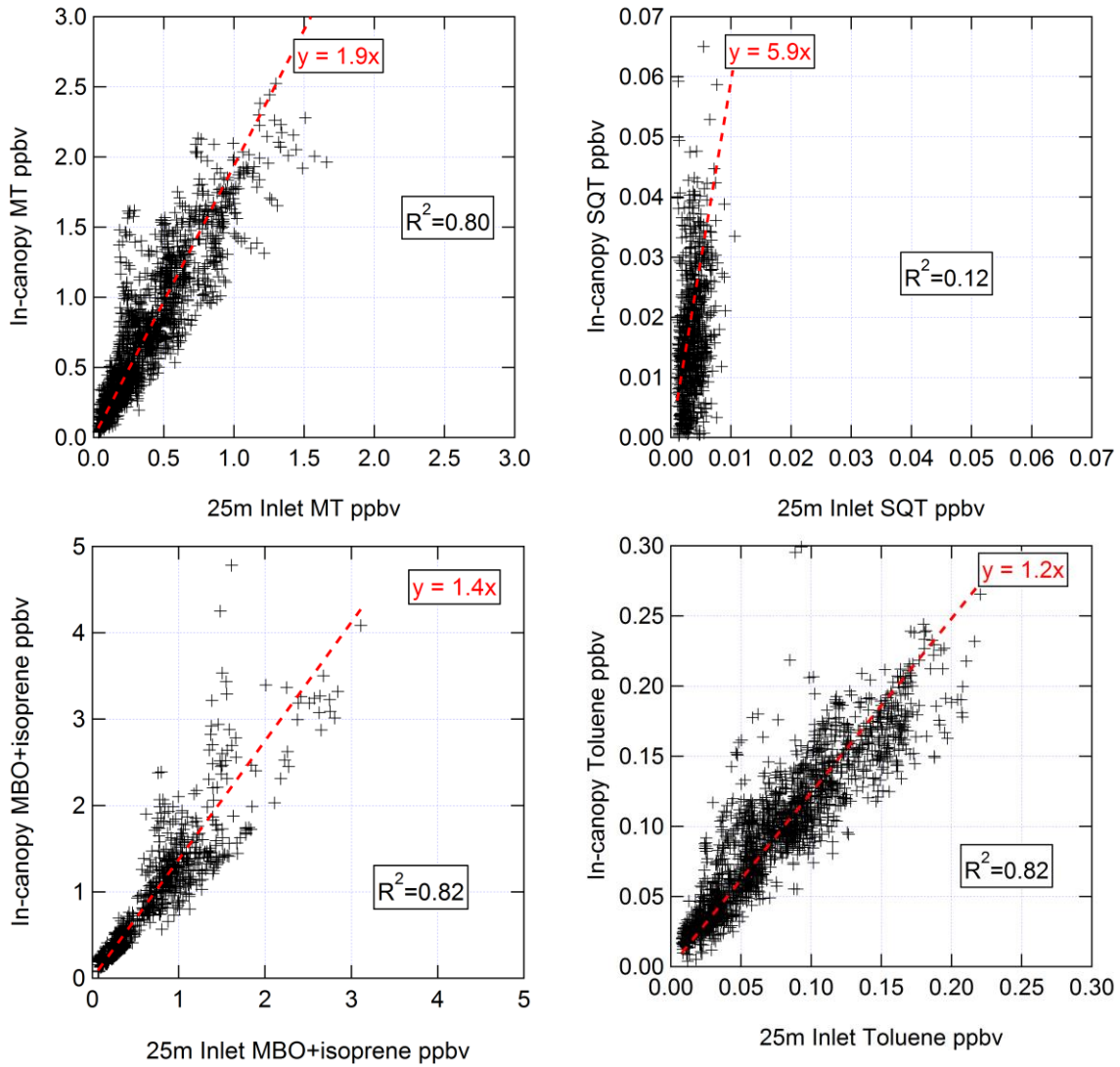
181
 182 Fig. S6. Scatter plot of aerosol volume and change in volume after OH aging from AMS vs. SMPS. AMS
 183 volume was estimated using densities of 1.52 g cm^{-3} for chloride, 1.75 g cm^{-3} for sulfate, ammonium, and
 184 nitrate (DeCarlo et al., 2004; Salcedo et al., 2006; Lide, 2013), and a parameterization using elemental
 185 composition to estimate the density of OA (Kuwata et al., 2012). Data is shown for base case
 186 (uncorrected) for particle transmission losses in the AMS aerodynamic lens according to Fig. S5. All data
 187 is shown without the LVOC fate correction. At the highest ages, heterogeneous oxidation led to
 188 fragmentation/volatilization of preexisting OA, resulting in a net loss of OA.



189

190 Fig. S7. Time series of ambient OA, total OA, and OA enhancement for OFR185 and OFR254 methods,
 191 ambient MT (25 m inlet), and ambient S/IVOC mass concentrations measured by the TD-EIMS. The OA
 192 enhancements are not LVOC fate corrected here, and include all ages.

193



194

195

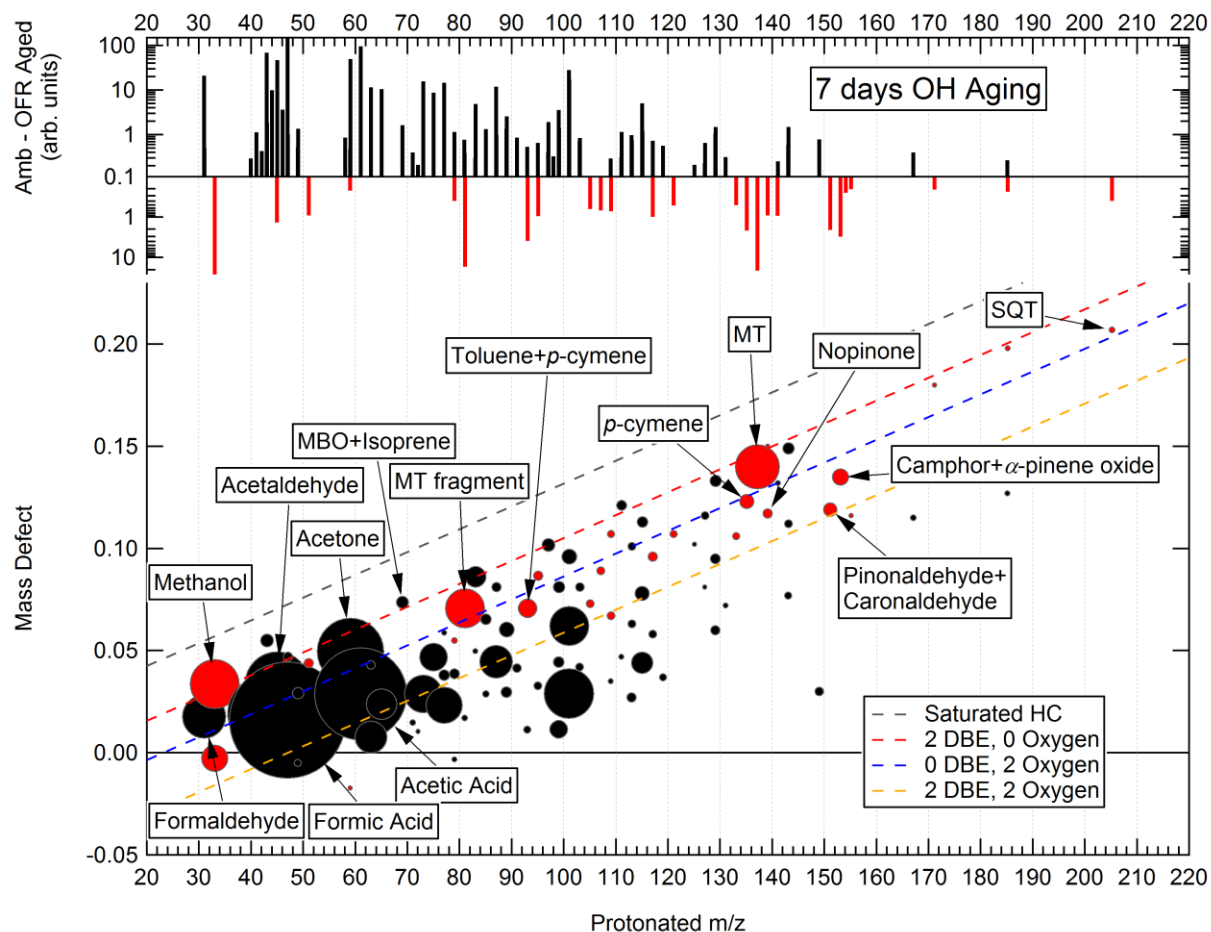
Fig. S8. Scatterplots of in-canopy (through OFR or 1 m inlet) vs. 25 m inlet for PTR-TOF-MS

196

measurements of MT, SQT, MBO+isoprene, and toluene. In-canopy concentrations were 1.9, 5.9, 1.4,

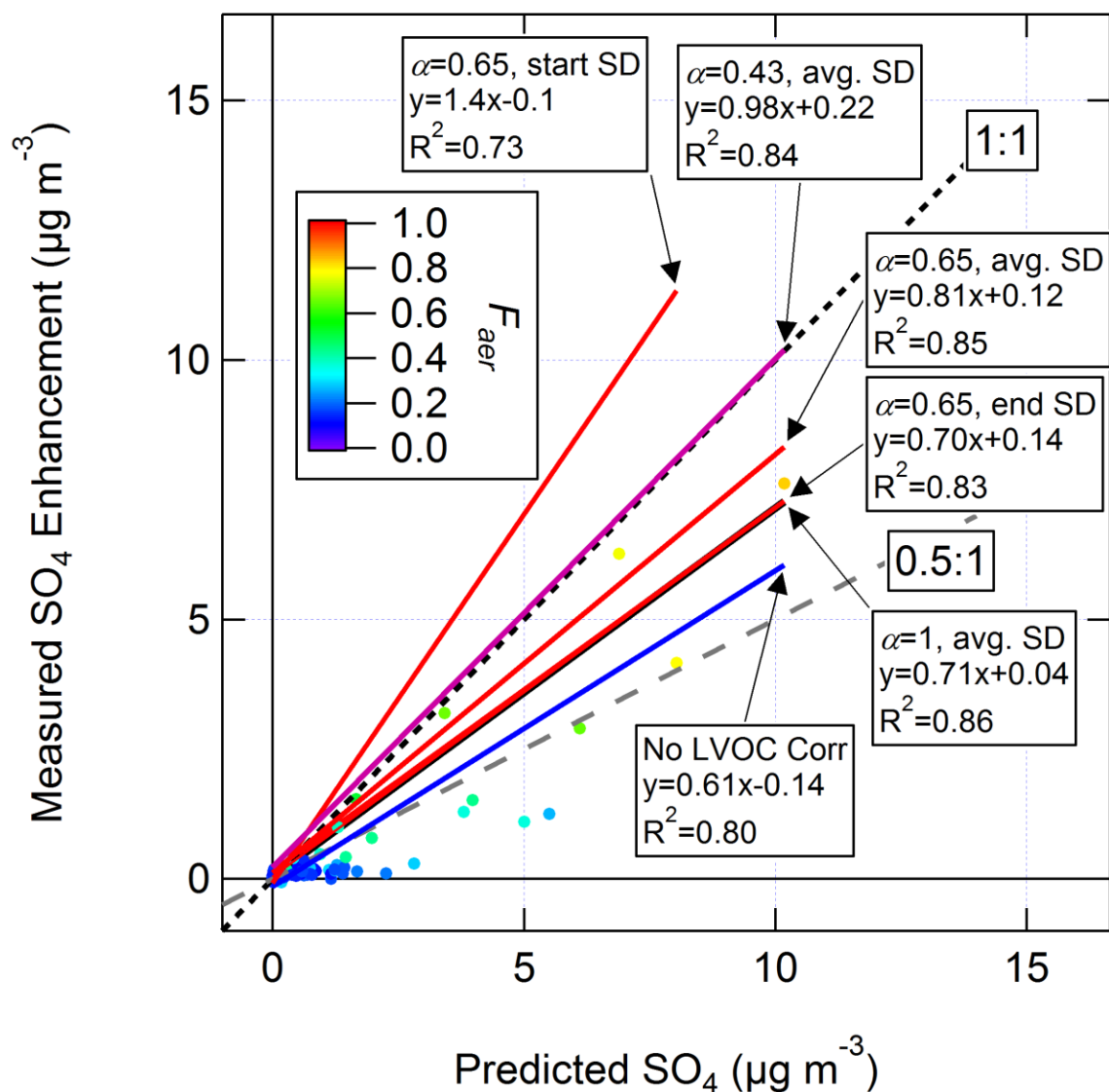
197

and 1.2 times higher than at 25 m, respectively.

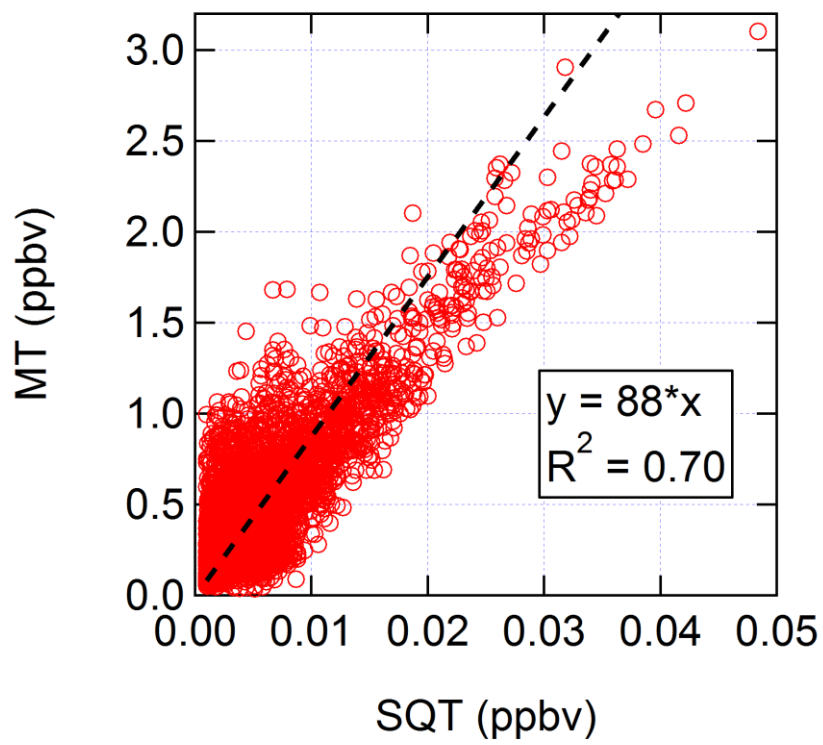


198

199 Fig. S9. The absolute changes of ions (signal after OH oxidation in the reactor minus ambient signal)
 200 measured by the PTR-TOF-MS after 7 days of aging using the OFR185 method, shown as a difference
 201 mass spectrum and in a mass defect diagram. The mass spectra are 10-min averages (5 min from each of
 202 the two sample cycles used). The background-subtracted signals are shown in arbitrary units, not
 203 corrected for differences in sensitivity of each compound due to the large number of compounds and
 204 the inability to positively identify all of them. Prominent ions are labeled by name or elemental formula
 205 assignments. Dashed lines representing molecules with varying double bond equivalents (DBE) or
 206 number of oxygen atoms are shown for reference. A red marker signifies that the signal decreased due
 207 to oxidation, while a black marker indicates where signal was greater after oxidation. The markers are
 208 sized by the square root of the absolute change in signal at each peak after oxidation (i.e., marker area is
 209 proportional to signal). Minor signals with absolute change of <0.2 arb. units or change of <20% of total
 210 ambient signal are removed.

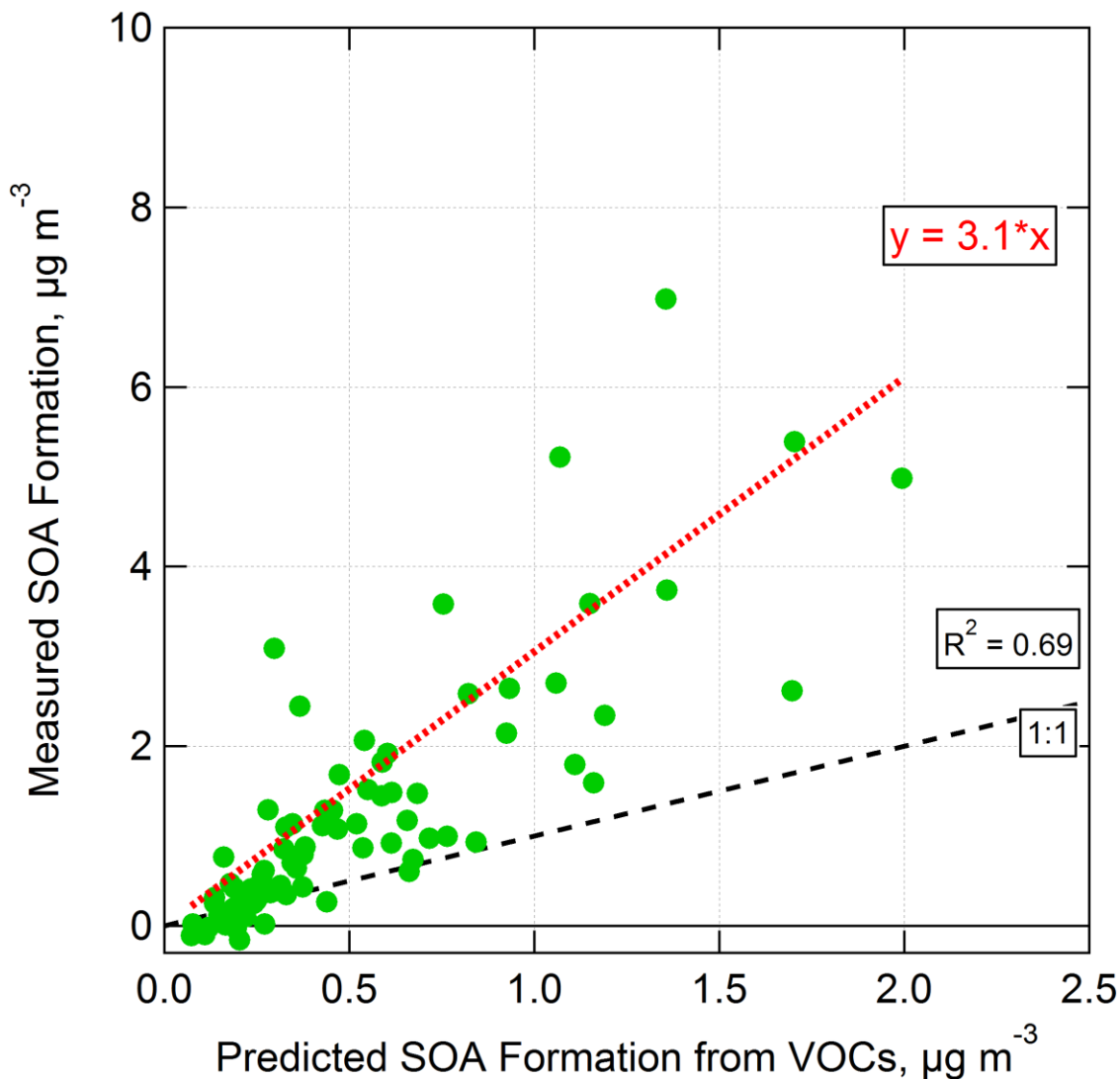


211
 212 Fig. S10. Sensitivity study of the measured vs. predicted SO_4 formation after OH oxidation in the OFR vs.
 213 key uncertain parameters. The data points are colored by the fraction of H_2SO_4 predicted to condense
 214 on aerosols, calculated using $\alpha = 0.65$ and the average of the SMPS size distributions (SD) measured
 215 before and after oxidation. Data are shown without applying the LVOC fate correction, along with linear
 216 fits that result from applying various sets of corrections including $\alpha = 0.43-1$ and using the ambient
 217 (start), post-oxidation (end), or average SD to calculate the CS. Ambient SO_2 concentrations <0.2 ppb
 218 have been excluded from this analysis.

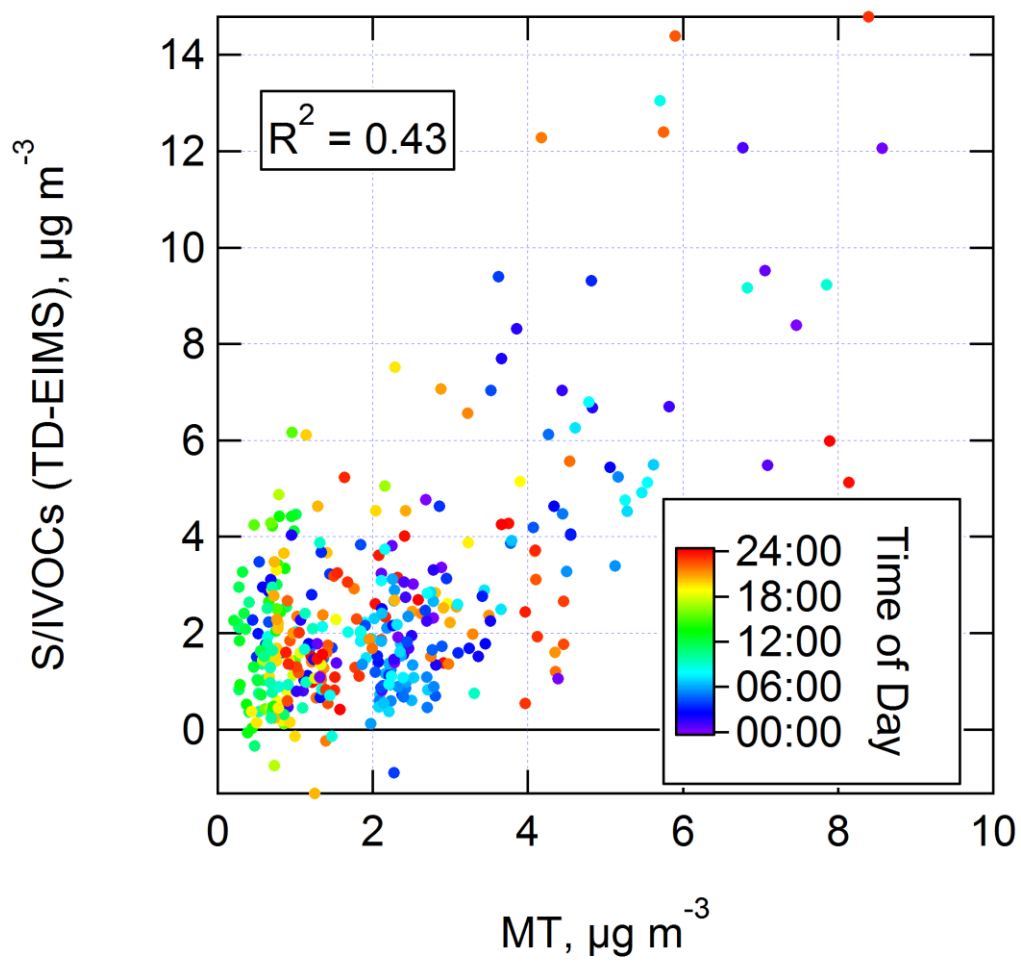


219

220 Fig. S11. Scatterplot of ambient MT vs. SQT concentrations measured by the PTR-TOF-MS at the 25 m
221 inlet above the canopy.



222
 223 Fig. S12. Measured vs. predicted SOA formation from OH oxidation of ambient air in an OFR using the
 224 OFR185 method. Only the range of photochemical ages with the highest SOA formation (0.4-1.5 eq.
 225 days) was used. The LVOC fate correction was not applied. Predicted SOA formation was calculated by
 226 applying OA concentration-dependent yields (average of 10.9%, 11.1%, 11.5%, and 2.9% for MT, SQT,
 227 toluene, and isoprene, respectively, with average OA concentration of $2.9 \mu\text{g m}^{-3}$) to VOCs reacted in the
 228 OFR (Tsimpidi et al., 2010). The amount of reacted VOCs was estimated using OH_{exp} and ambient VOC
 229 concentrations. If a non-zero y-intercept is allowed, the regression line becomes $y = 4.0x - 0.8$.



230

231 **Fig. S13.** Scatterplot of mass concentration of ambient S/IVOCs (lower limit measured by TD-EIMS) vs.
 232 ambient MT measured by PTR-TOF-MS. Data are shown colored by local time of day.